A Bi-Specific T Cell-Engaging Antibody Shows Potent Activity, Specificity, and Tumor Microenvironment Remodeling in Experimental Syngeneic and Genetically Engineered Models of GBM.

Markella Zannikou [1&], Joseph T. Duffy [1&], Daniele Procissi[3], Rebecca N. Levine [1], Dolores Hambardzumyan[4], Catalina Lee-Chang [1], Lara Leoni [3], Bin Zhang [2], Jason M. Miska [1], Irina V Balyasnikova [1*].

[&] Equally contributed to this work

[1]*Department of Neurological Surgery, Feinberg School of Medicine, Northwestern University, Chicago, Illinois.*

[2]*Department of Medicine, Feinberg School of Medicine, Northwestern University, Chicago, Illinois.*

[3]*Department of Radiology, Feinberg School of Medicine, Northwestern University, Chicago, Illinois, USA.*

[4]*Department of Pediatrics, The Tisch Cancer Institute, Mount Sinai Icahn School of Medicine, New York, NY, 10029, USA*

Keywords: Bi-specific T cell-engagers, glioblastoma, targeting, immunotherapy, and interleukin 13 receptor alpha 2

Running title: Bi-specific T cell engaging protein demonstrates potent therapeutic properties in murine glioma models

[*]**Corresponding Author:**

Irina V. Balyasnikova, Ph.D.
Northwestern University Feinberg School of Medicine,
303 E. Superior Street, Suite 3-313,
Chicago, IL 60611
Phone: 312-503-48-68
Fax: 312-695-4075
E-mail: irinabal@northwestern.edu

ABSTRACT

Background. Bispecific T cell-engagers (BTEs) are engineered antibodies that redirect T cells to target antigen-expressing tumors. BTEs targeting various tumor-specific antigens, like interleukin 13 receptor alpha 2 (IL13RA2) and EGFRvIII, have been developed for glioblastoma (GBM). However, limited knowledge of BTE actions derived from studies conducted in immunocompromised animal models impedes progress in the field. To close this gap, we investigated how BTE functions, engaging hosts' immune systems in the context of the immunosuppressive tumor microenvironment (TME) of the orthotopic and genetically engineered pre-clinical models of GBM.

Methods. We developed a BTE protein that bridges CD3 epsilon on murine T cells to IL13RA2-positive GBM cells. We then investigated the BTE therapeutic mechanism to promote anti-glioma activity in immunocompetent mouse models of GBM. To do so, we paired survival studies with multi-color flow cytometry, multiparametric magnetic resonance imaging (MRI), and single-cell RNA sequencing (RNA-Seq) in several orthotopic and genetically engineered mouse (GEM) models of GBM.

Results. BTE-mediated interaction of murine T cells and GBM cells potently activated T cells, resulting in antigen-dependent killing of GBM cells. BTE treatment significantly extended the survival of mice bearing IL13RA2-expressing orthotopic glioma and *de novo* formed GBM in the GEM model. The quantification parametric MR imaging validated the survival data, showing a reduction in tumor volume and decreased tumor viability. Flow cytometric and scRNA-seq analyses of the tumor microenvironment (TME) revealed robust increases in activated and memory T cells and decreases in immunosuppressive myeloid cells in the brains of mice following BTE treatment.

Conclusions. Our data demonstrate that BTE's survival benefits in GBM are due to its ability to engage the host immune system in direct killing, boost immunological memory, and modulate the TME. These findings provide a deeper insight into the mechanism of BTE actions in GBM.

INTRODUCTION

Glioblastoma (GBM) is an aggressive and incurable brain tumor with a poor prognosis [1]. The current standard of care for primary disease involves surgical resection, followed by radiation therapy and chemotherapy with the alkylating agent temozolomide [2]. Despite significant advancements in both preoperative and intraoperative technologies, such as cortical mapping and stereotactic navigation, as well as progress in radio-oncology techniques like modulated proton therapy and fractionated stereotactic radiosurgery, tumor progression remains nearly inevitable. Consequently, median overall survival remains under 15 months, and the 5-year survival rate at less than 5% [3, 4]. There is still no standard of care for recurrent disease, forcing patients to choose between experimental trials or additional interventions. This prognosis underscores the urgent need for novel therapies to enhance survival outcomes in GBM.

The success of T cell-based immunotherapeutic treatments in hematopoietic malignancies has gained considerable recognition in recent years. Among them are Bi-specific T cell engagers (BTEs), a class of engineered bispecific antibodies with potent anti-cancer properties. BTEs consist of two single-chain variable fragments (scFvs) derived from different monoclonal antibodies fused by a peptide linker. One of BTE's scFv recognizes a T cell stimulatory receptor, such as Cluster of Differentiation 28 (CD28) or CD3 epsilon (CD3E) subunit of the T-cell receptor complex; the other scFv is specific for a tumor antigen. In bridging T and tumor cells, BTEs activate T cells and direct T cell-mediated killing of malignant cells. Unfortunately, the progress in propelling BTE therapy for solid tumors has been limited. GBM is regarded as among the most challenging tumors to treat due to the blood-tumor barrier limiting penetration of therapeutics into the tumor, immune-suppressive environment, heterogeneous expression of tumor-associated antigens, and limited T cell presence within the tumor bed [5]. Nonetheless, the development of BTEs continues to gain traction in GBM. Our group has previously shown the efficacy of BTE targeting the glioma-associated antigen interleukin 13 receptor subunit alpha 2 (IL13RA2) in preclinical patient-derived xenograft (PDX) models of GBM. Others have demonstrated a significant therapeutic effect of BTE targeting EGFRvIII, a glioma-specific antigen, in PDX models of GBM, and a clinical study evaluating this BTE's safety is anticipated (NCT04903795). However, these preclinical studies were carried out using immunocompromised hosts, and the lack of a functioning immune system within these models renders them unable to recapitulate the highly immunosuppressive TME in human GBM [6].

As strategies to overcome the blood-tumor barrier[7] and develop BTEs with varying target specificities continue to advance[8-12], gaining a deeper understanding of the mechanistic actions of BTEs in fully immunocompetent GBM models is crucial for informing future clinical study designs. Therefore, we designed this study to investigate the therapeutic mechanisms of BTEs in orthotopic and genetically engineered GBM models in mice with intact immune systems. Our findings demonstrate that the activation of murine T cells depends on BTE's binding to its target, IL13RA2, both in vitro and in vivo. Moreover, we observed that BTE treatment increases the proportion of activated T cells within the tumor and leads to a higher

frequency of memory T cells in the tumors and brains of long-term surviving mice. These results suggest that BTE engagement with the host immune system enhances BTE's therapeutic efficacy against glioma cells.

MATERIAL AND METHODS

Cell culture

GL261-IL13RA2, CT2A-IL13RA2, and SMA-560-IL13Rv2 were modified with human IL13RA2 as previously described [13]. Glioma cell lines were cultured in Dulbecco's Modified Eagle Medium (DMEM) (Corning Life Sciences; Corning, NY; Cat No. 10-013-CV) supplemented with 10% v/v fetal bovine serum (FBS) (R&D Systems; Minneapolis, MN; Cat. No. S11550) and 1% v/v Penicillin-Streptomycin (PS) (Corning Life Sciences; Cat No. 10-013-CV). Cell lines were screened for mycoplasma via the MycoAlertTM Mycoplasma Detection Kit (Lonza, Walkersville, MD; Cat No. LT07-318).

Generation of BTE and Binding Studies

BTE molecule consisting of two single-chain variable regions (scFv) of antibodies, scFv145-2C11 (against murine CD3 epsilon subunit of T-cell receptor complex; CD3e)[14] and scFv47 (against human IL13RA2)[15, 16], connected through a 23aa Gly_4S flexible linker, was synthesized by GenScript (Piscataway NJ) and subcloned in a pLVX-IRES-zsGreen 1 (Takara Bio, Mountain View, CA; Cat. No. 632187) lentiviral expression cassette. The BTE molecule in which the CDR3 of the scFvIL13RA2 light chain was replaced by the CDR3 domain of a non-specific antibody MOPC-21 (named NC-BTE) to generate as a negative control protein lacking the interaction with IL13RA2. For the production of soluble BTE proteins, HEK293T cells were transduced with lentiviral particles. Proteins were isolated from the supernatants using His-Tag affinity chromatography, as previously described[17], and characterized for their size and binding specificity against IL13RA2 by Western Blot and ELISA.

Western Blot and ELISA

Western and enzyme-linked immunosorbent assay (ELISA) were carried out as previously described [17]. Briefly, Pierce™ BCA Protein Assay Kits (ThermoFisher Scientific, Waltham, MC; Cat. No. A55864) was used, per manufactural protocol, to quantify purified BTE and NC-BTE concentration prior to western blot and ELISA. For western blot analysis, purified protein samples were then diluted into Laemmli Sample Buffer (Bio-Rad, Hercules, CA; Cat. No. 1610747) supplemented with 2.5% beta-mercaptoethanol (Sigma Aldrich, St. Louis, MO; Cat. No. M6250) and heat-denatured for 10 min at 95°C. Samples and 250 kDa Precision Plus Protein standard (Bio-Rad Laboratories, Cat No. 1610375) were then separated by size via SDS-polyacrylamide gel electrophoresis (SDS-PAGE) using a 4-20% Midi-PROTEAN® TGX Stain-Free™ gel (Bio-Rad Laboratories; Cat. No. 17000436). Trans-Blot® Turbo Transfer System™ (Bio-Rad Laboratories) was used to transfer separated proteins onto a methanol-activated 0.2 µm PVDF membrane (Millipore Sigma, Burlington, MA; Cat. No. IPVH08100). Membranes were blocked for 2 hours at RT with 5% non-fat dry milk (NFDM) in tris buffered saline-tween-20 (TBST) (Boston Bioproducts, Ashland, MA; Cat #IBB180), incubated at RT for 2 hours with HRP Anti-6X His tag® antibody (1:1000) (Abcam, Cambridge, United Kingdom; Cat. No.

AD1.1.10), washed with TBST, incubated with Clarity™ Western ECL Substrate (Bio-Rad Laboratories; Cat. No. 1705061), and visualized via chemiluminescent imaging using ChemiDoc™ MP Imaging System (Bio-Rad Laboratories). For ELISA, 96 well plates were coated with 1 μg/mL of recombinant IL13RA2hFc (R&D Systems, Minneapolis, MN, Cat No. 7147-IR-100) and IL13RA1hFc (R&D Systems, Minneapolis, MN, Cat No. 146-IR-100). Plates were blocked with 2% bovine serum albumin (BSA) in TBST, washed thrice with TBST, incubated with various dilutions of BTE and NC-BTE. Plates were then incubated with for two hours with Anti-6X His tag® antibody (1:1000) (Abcam; Cat. No. AD1.1.10), washed 5 times with TBST, and incubated with 1- Step™ Slow TMB-ELISA (Thermo Scientific; Cat. No. 34022) and 2N HCl per manufactures protocol. BTEs were quantified via a colorimetric readout at 470 nm using a BioTek plate reader (BioTek, Winooski, VT).

Chromium-51 (Cr^{51}) Release Assay

Chromium-51 (Cr^{51}) release assays were used to assess BTE-induced T cell-mediated cytotoxicity against glioma cells. Briefly, splenic murine t cells were isolated from C57BL/6 mice using EasySep™ Mouse T Cell Isolation Kit (STEMCELL Technologies; Cat. No. 19851). Glioma cells were labeled with Cr^{51} (0.05 mCi) (Revvity, Waltham, MA; Cat No. NEZ030001MC). Murine T cells were then co-cultured with labeled glioma cells at a 20:1 E:T ratio and treated with various concentrations of BTE protein. The positive control consisted of Dynabeads™ CD3/CD28-activated T cells (GIBCO, Waltham, MA; Cat11452D). Following 18 hours, supernatants were carefully removed, placed into 96 well LumaPlate-96 (PerkinElmer; Wellesley; MA Cat No. 6006633), dried via evaporation, and Cr^{51} activity was measured in a gamma counter (PerkinElmer; Wellesley; MA). Specific lysis was computed relative to spontaneous and maximum (measured via target cell incubation with 1% Triton X-100). Data was displayed as SEM of triplicates; statistical significance was denoted via *p*-value from student t-test.

Orthotopic Xenograft and Genetically Engineered Mouse Model

All animal experiments performed were in accordance with Northwestern University Institutional Animal Care and Use Committee approved protocol IS00016555. Orthotopic models utilized CD45.1 and C57Bl/6 mice, sourced from Jackson Laboratories, and VMDK mice provided by Dr. J. Sampson (Duke University). The *de novo* GEMM glioma model employed nestin-TvA PTENfl/fl p53fl/fl mice, generously gifted by Dr. O. Becher (Mount Sinai).

In all models, tumors were established via stereotactic injection of either murine glioma cells (orthotopic model) or DF-1 viral-producing cells (GEM model) into the cerebral cortex, approximately 1 mm posterior to the bregma and 1 mm to the right of the midline, as previously described [13]. Mice were randomized by gender into treatment groups: BTE, NC-BTE, or

saline. Treatments were administered intraperitoneally (i.p.) 4 days per week, starting 7 days post-tumor implantation and continuing for three weeks. Mice were monitored for survival, with endpoints defined as either a 20% reduction in body weight or the onset of neurological symptoms.

Flow Cytometry

All in vitro and in vivo flow cytometric staining followed a standardized operating procedure (SOP). Cells were blocked with Dulbecco's Phosphate-Buffered Saline (DPBS) (Corning Life Sciences; Cat. No. 20-031-CV) supplemented with 2% FBS (R&D Systems) and TruStain FcX™ anti-mouse CD16/32 (1:200; BioLegend, San Diego, CA; Cat. No. 101319). Surface antigens were stained using fluorochrome-conjugated antibodies in 2% FBS-DPBS for 20 minutes on ice. Dead cells were labeled with eBioscience Fixable Viability Dye eFluor 780 (1:1000 in DPBS; Invitrogen, Waltham, MA; Cat. No. 65-0865-18). Cells were fixed and permeabilized with the eBioscience™ FOXP3/Transcription Factor Staining Buffer Set (Invitrogen; Cat. No. 00-5523-00), followed by intracellular staining with fluorochrome-conjugated antibodies. Data acquisition was performed using the BD FACSymphony A5-Laser Analyzer (Becton Dickinson, Franklin Lakes, NJ) at the Robert H. Lurie Comprehensive Cancer Center (RHLCCC) Flow Cytometry Core Facility. Flow cytometric analyses were conducted using FlowJo v10.9.0 software (Becton Dickinson). A complete list of antibodies and their respective concentrations is provided in Supplementary Table 1.

For *in vitro* T cell activation experiments, splenic murine T cells were freshly isolated from C57BL/6 mice using the EasySep™ Mouse T Cell Isolation Kit (STEMCELL Technologies, Vancouver, Canada; Cat. No. 19851) following the manufacturer's protocol. Murine T cells were co-cultured with glioma cells at a 20:1 effector-to-target (E:T) ratio in triplicate wells of a 96-well plate and treated with various concentrations of BTE, NC-BTE, or Dynabeads™ Mouse T-Activator CD3/CD28 (Gibco, Carlsbad, California; Cat. No. 11456D) for 24 hours. Following incubation, cells were collected for flow cytometric staining.

For *in vivo* tumor microenvironment analysis, tumors were implanted as described under the Orthotopic Xenograft Mouse Model. Mice were randomized into BTE, NC-BTE, or saline groups, and treatments were administered intraperitoneally (i.p.) starting 7 days post-tumor implantation. Brains and spleens were harvested 48 hours after the final treatment, mechanically dissociated into single-cell suspensions using a 70 µm cell strainer, counted using trypan blue exclusion, and processed for flow cytometric staining.

Incucyte

For *in vitro* T cell activation experiments, we utilized splenic murine T cells of NOD.Nr4a1GFP/Cre mice (Jackson Laboratory, Milwaukee; RRID:IMSR_JAX:037122) as reporter assay to visualize BTE-mediated T cell activation. Nr4a1 is a transcription factor downstream of TCR signaling. NOD.Nr4a1GFP/Cre mice contain a cre recombinase/green

fluorescent fusion protein driven by the Nr4a1 (also known as Nur77) promoter. Thus, NOD.Nr4a1GFP/Cre T cells begin to express GFP following activation. Briefly, murine T cells were freshly isolated from NOD.Nr4a1GFP/Cre mice using the EasySep™ Mouse T Cell Isolation Kit (STEMCELL Technologies; Cat. No. 19851) per manufacturer's protocol. These murine T cells were then co-cultured with Gl261-IL13RA2 glioma cells at a 20:1 E:T ratio and treated with either of BTE, NC-BTE, or Dynabeads™ Mouse T-Activator CD3/CD28. In total, mean fluorescent intensity at excitation of 488 nm was quantified from 12 images obtained between 0.75 and 18 hours post-treatment.

Histology

The protocol for detecting immune cells in the murine brain of the adult GEM model has been previously described (Seblani et al., doi.org/10.1101/2021.10.15.464284). The following antibodies were used: IL13RA2 (R&D Systems, Cat No. AF146), Olig2 (Abcam, ab109186), Ki67 (Abcam, ab16667), CD3 (Abcam, ab16669), and CD11B (Abcam, ab133357). For the detection of $CD8^+$ T cells in the brains of LTS mice, 4% paraformaldehyde (PFA)-fixed paraffin-embedded 4 μm thick-tissue section from the mouse brains were incubated with the CD8a monoclonal antibody (4SM16) (Invitrogen, 14-0195-82), followed by 3,3′-diaminobenzidine (DAB) chromogen staining. The quantification of the stained areas was performed using the ImageJ software. The tissue was stained with hematoxylin and eosin (H&E) to highlight the morphological changes, and the image analysis was performed using the NDP.view 2.8.24 software (Hamamatsu Photonics K.K.).

Magnetic Resonance Imaging

Magnetic resonance imaging of tumor-bearing mice was conducted on control and BTE-treated mice using a Bruker Clinscan 7T MRI equipped with a dedicated multi-channel brain coil for high sensitivity and high spatial resolution acquisition of whole-brain images. Advanced Siemens MR sequences (Syngo VB15 Imaging platform, Siemens) were used to obtain several types of whole-brain images with technical acquisition and spatial parameters, as listed below. Anesthesia was delivered via a built-in MRI holder nose cone (100%Oxygen mixed with isoflurane), and appropriate physiological conditions (i.e., body temperature and respiration rate) were maintained throughout each scanning session using the dedicated physiological monitoring and control system (Sai Instruments, NJ). Anatomical whole-brain 3D T1-Weighted images with ~ 100-micron isotropic spatial resolution were obtained using a FLASH-based 3D gradient-echo sequence with TR=100 msec and TE=3 msec. 2D quantitative multiple echo-times spin-echo sequence (TR= 1500 msec and 12 echo times TE ranging from 10-120 msec) was used to acquire whole-brain images. Following the acquisition, DICOM images were exported to Northwestern Feinberg Medical School cloud-based repository (FSMresFiles Server) and processed using a

combination of shareware and commercial imaging software (Jim7.0 Xinapse, ITK_SNAP). T2 maps were extracted by fitting the multiple sets of images with different echo-times on a voxel-by-voxel using a least-square fitting tool included in JIM7.0 Xinapse image processing software with the expectation of using the regional quantitative variability of the extracted maps as a marker of intratumor BiTE-induced effects. A regional semi-automated threshold-based segmentation tool included in ITK-SNAP software was used to extract 3D whole-tumor volumetrics. Tumor quantitative T2 parametric maps were normalized using T2 values from normal (i.e., no tumor) brain tissue. The resulting T2tumor /T2tissue normalized parametric maps were then analyzed using a threshold-based approach, which consisted of using defined quantitative threshold windows (from high vs low T2tumor /T2tissue values). The resulting segmented regions corresponding to different ranges of T2tumor /T2tissue values were color-coded, providing a spatial representation of tumor microenvironment regions with different biological properties. This approach allows us to identify and use a robust non-invasive imaging metric that has the potential, when compared with the corresponding histopathological analysis conducted ex vivo on the same tumors, to facilitate interpretation of the different tumor subregions (i.e., different tumor habitats), which are reflective of different stages of progression/viability. The volume of each sub-region (i.e., regions with specific average T2tumor /T2tissue values) for each mouse was used to generate quantitative dimensional parameters (using whole brain volume as a normalization factor) that were used for statistical analysis. Specifically, we computed and compared the average indexes for the control and the BTE-treated group for the high and low T2 ranges.

Based on existing preclinical and clinical reports suggesting the predictive diagnostic potential of regional intra-tumor T2 values, we extracted and calculated a quantitative dimensional parameter (i.e. volumetric ratios) that could potentially be used as a non-invasive biomarker of tumor progression and/or response to therapy. We defined such parameter as the Tumor therapeutic response index and calculated it as shown in equation 1 below by dividing the volume corresponding to tumor regions with low to intermediate values of T2 by the total tumor volume for each mouse (as shown in equation 1 below). The driving hypothesis is that lower tumor tissue T2 values tend to be detected (clinically and pre-clinically) in less active or therapeutically more responsive tumors, thus leading to consistently high Tumor Therapeutic Response Index values in three BTE mice compared to the control.

EQ1 Tumor Therapeutic Response Index: Volume Low Range T2tumor / T2tissue / Volume Whole Brain

Single Cell RNA Sequencing

We performed single-cell RNA sequencing (siRNA seq) of control and BTE-treated *de novo* tumors derived from Nestin-Tva-PTENfl/fl-P53fl/fl mice in two independent experiments with identical designs. In both experiments, gliomagenesis was induced by p53 and PTEN deletion

using DF1 cells producing RCAS-cre and by inserting PDGFB and IL13RA2 using RCAS-PDGFB-IL13RA2 virus as previously described [18]. We then randomized mice evenly by gender into two groups, with 5 mice per group. Seven days post tumor induction, we treated mice with either saline or BTE (10mg/kg) via intraperitoneal (i.p.) route four times per week for 3 weeks. Forty-eight hours after the last treatment, we anesthetized mice and perfused intracardially with 10 ml of saline, excised tumor tissue, and obtained single-cell suspension using the Adult Brain Dissociation Kit, Mouse and Rat (Miltenyi Biotec, Gaithersburg, MD; Cat No. 130-107-677) per manufacturer protocol. We then incubated single-cell suspensions with anti-CD16/32 (Fc Block) antibodies (BioLegend) and subjected them to anti-mouse CD45 bead-based separation (Miltenyi Biotec; Cat. No 130-052-301) per manufactural protocol. The final cell suspension we performed scRNA-seq on consisted of tumor-infiltrating immune cells enriched at a CD45+ to CD45- cell ratio of 8:2 at a 4000 live cells/µL concentration.

We used PIPseq™ T2 3' Single Cell RNA Kit v4.0 kit (Fluent Biosciences, Cat No. FBS-SCR-T20-4-V4.05) to perform scRNA-seq per manufactures protocol. PIPseq uses a microfluidics-free, templated emulsification technology to generate monodispersed cell droplets. Briefly, we added 4×104 cells per sample to particle-templated instant partitions, emulsified them via rapid mechanical vortexing, lysed them to capture mRNA on barcoded poly(T) decorated beads, reverse transcribed them into cDNA, amplified them via PCR, and sample indexed them with unique P7 and P5 Illumina compatible indexes. We subjected the barcoded cDNA libraries to pooled sequencing on an Illumina NovaSeq X Plus at a depth of 650 million reads per sample at Novogene (Sacramento, CA).

We aligned demultiplexed FASTq files to the Human Hg38 genome assembly (GRCh38.p13, 2022) using the PIPseeker (Fluent BioSciences) software and analyzed the resulting data matrix files for each sample in R (v4.2.3) using Seurat (v5) package. Briefly, we filtered cells with>2.5% mitochondrial read counts with >500 expressed genes and used scDblFinder (v1.18.0) to identify and remove doublets. In Seurat, we first log normalized data using a scale factor of 10,000. We then used default parameters to identify highly variable genes and subsequently performed principal component analysis (PCA) using the top 2000 variable genes. We used the top 17 PCs for neighboring and clustering identification. To correct the batch effect between the two experiments, we performed canonical correlation analysis (CCA), subsequently used the JoinLayers function to merge sample layers, and used the top 17 CCA dimensions for neighboring and clustering identification. We visualized the clusters in Uniform Manifold Approximation and Projection (UMAP) of the first 17 CCA reductions, used FindAllMarkers to find top differentially expressed genes between clusters, and identified cell types based on canonical markers. We used standard Seurat workflow to subcluster the T NK cell cluster and FindMarkers function to identify differentially expressed genes (DEGs) between Saline and BTE-treated samples. We then used ClusterProfiler (v4.12.0) was to perform gene ontology enrichment analysis on significant DEGs. We used the R packages ggplot2 (v3.5.1) and ComplexHeatmap (v2.20.0) to make plots and heat maps.

Statistical analyses.

All statistical analysis was completed in R (v4.2.3). Statistical analys performed by one-way ANOVA, and p values were adjusted for multiple comparisons using Tukey's test. Curve comparison of two groups for survival analyses was performed by log-rank (Mantle-Cox) test, and p values were adjusted for multiple comparisons by Bonferroni's correction.

RESULTS

Generation and Functional Characterization of CD3xIL13RA2 BTE.

Single-chain variable fragments (scFv) derived from the monoclonal antibody 2C11-145 binding murine CD3e[14] and the monoclonal antibody against human IL13RA2 (clone 47)[15, 16] were used to generate a BTE protein suitable for studies in an immunocompetent host. The two scFv were genetically linked with a 23 amino acids GlyS linker[17]. We generated a negative control BTE (NC-BTE) protein by aligning and replacing the unmatched amino acids in the CDR3 domain of VL scFv targeting IL13RA2 with those from the scFv p588 sequence, previously established negative control antibody (MOPC1) as previously described[17]. Constructs were generated by subcloning codon-optimized cDNA encoding BTE and NC-BTE in pLVX-IRES-ZsGreen1 lentiviral constructs **(Fig. 1A)**. To produce BTE proteins, 293T cells were transduced with BTE and NC-BTE constructs and subsequently flow-sorted to enrich for the cells with the brightest ZsGreen1 positive 293T cells. Western blot of purified BTE showed a protein with an anticipated molecular weight of about 55 kDa (**Fig. 1B**). The specificity of BTE to IL13RA2 was confirmed in plate ELISA, where BTE, but not a negative control NC-BTE, interacted with recombinant IL13RA2 (Fig. 1C). No binding of BTE with IL13RA1 was detected, thus further confirming its specificity to IL13RA2 (Fig. 1C).

Next, we tested the ability of BTE to activate T cells and direct T cell-mediated killing of murine glioma cells *in vitro*. We utilized murine glioma cell lines GL261, SMA560, and CT2A previously modified to express IL13RA2[13]. T cell activation was assessed via flow cytometry, and cell-mediated killing was assessed via Cr^{51}-release assay; T cells activated with CD3/CD28/CD2 immuno-beads served as a positive control. The BTE, but not NC-BTE, significantly increased the killing of SMA560-IL13RA2 and GL261-IL13RA2 cells in a dose-dependent manner (**Fig 1.D**). BTE also induced significant expression of early activation maker CD69 observed in CD8+ T cells upon engagement with SMA560-IL13RA2, GL261-IL13RA2, and CT2A-IL13RA2 cell lines (**Fig. 1E**). Collectively, this data validates we generated functional BTE and corresponding negative control NC-BTE protein suitable for studies in immunocompetent syngeneic models of glioma.

Treatment with BTE Enhances Survival and Modulates Tumor Microenvironment of Mice Bearing IL13RA2-expressing Glioma.

Following functional confirmation *in vitro*, we set to investigate the biological function of BTE *in vivo* using a syngeneic disease model of glioma. To assess the penetration of BTE into the brains of GL261-IL13RA2 tumor-bearing mice, we administered AF647-labeled BTE intravenously via the tail vein and performed dynamic live fluorescent imaging. BTE was detected in the brains of tumor-bearing mice at various time points, with the signal intensifying between 3-6 hours post-injection and diminishing between 24-72 hours (**Fig.2A**).

Next, we conducted a titration experiment on SMA.560-IL13RA2 tumor-bearing mice treated with BTE (**Supp Fig.2A**). Mice were treated with BTE at 50 ug/mouse or 200 μg/mouse or

saline on 7, 9 and 11 post tumor implantation and followed for survival (**Supp Fig.2A**). Both doses of BTE significantly extended survival of mice compared to saline (MS=15, n=8), with both dosages of BTE producing 1 mouse surviving long-term (LTS) (**Supp Fig.2A**). No statistical difference in survival was seen between 50 ug/animal (MS=18, n=8) and 200 ug/animal (MS=27.5, n=8) (**Supp Fig.2A**). To confirm antigen specificity for our BTE molecule, we conducted a separate survival experiment in parental SMA.560 tumor-bearing mice, and observed no increase in survival between BTE, NC-BTE, and saline groups (**Supp Fig.2B**). From these results, we then conducted a survival analysis on SMA.560-IL13RA2 tumor-bearing mice treated with either BTE at 200 ug/animal, NC-BTE at 200 ug/animal, or saline (**Fig 2B**). Mice were treated on days 7, 9, and 11 post-tumor implantation and followed for survival. No difference in the median survival (MS) was seen between saline (MS=17, n=7) and NC-BTE (MS=19, n=8) (**Fig.2B**). BTE significantly extended the survival of mice (MS=33, n=7), with 40% of BTE treated mice reaching LTS (**Fig.2B**). Similar survival benefits from BTE treatment in a different model of murine glioma was observed in a separate experiment of CT2A-IL13RA2 bearing mice (**Supp Fig.2B**). To better understand how BTE affects the immune composition of the TME, we repeated this experiment in SMA.560-IL13RA2 tumor-bearing mice but sacrificed mice 3 days after the last dose of either BTE (n=5) or NC-BTE (n=5) (**Fig.2C**). We then processed the brains into single cell suspensions, stained the cells with fluorochrome-conjugated antibodies against canonical immune cell markers, and performed multi-color flow cytometric analysis (**Fig.2D-L**). We observed and increased frequency of T regulatory ($CD45^+CD4^+FOXP3^+$; p.adj=0.040)(**Fig.2E**), $CD8^+$ T cells ($CD45^+CD8^+$; p.adj=0.039)(**Fig.2F**), tissue resident memory $CD8^+$ T cells ($CD45^+CD8^+CD127^{hi}CD103^+$; p.adj=0.009)(**Fig.2H**), memory-like $CD8^+$ T cells ($CD45^+CD8^+CD127^{hi}$; p.adj=0.023)(**Fig.2I**), and monocytic myeloid derived suppressor cells (Mo.MDSC)($CD45^+CD11B^+CD11C^-LY6G^-LY6C^+$; p.adj=0.050)(**Fig.2J**), with a trending decrease in short-lived memory $CD8^+$ T cells ($CD45^+CD8^+CD127^{lo}KLRG1^+$; p.adj=0.102)(**Fig.2G**), polymorphonuclear MDSC (Pmn.MDSC)($CD45^+CD11B^+CD11C^-LY6G^+LY6C^-$; p.adj=0.080) (**Fig.2K**), and dendritic cells (DC)($CD45^+CD11B^+CD11C^+$; p.adj=0.159)(**Fig.2L**).

To understand changes in the tumor infiltrating T cell compartment, we profiled tumor and splenic immune compartment of CT2A-IL13RA2 bearing mice using flow cytometry **(Supp. Fig. 2D)**. Similar to experiments in SMA.560-IL13RA2 model, we observed a significant increased frequency of T regulatory cells in the brain following BTE treatment (p.adj=0.039), but not in the spleen (**Supp. Fig. 2E**). We analyzed markers of T cell cytotoxicity and activation and found increased expression of GZMB (p.adj=0.006) (**Supp. Fig. 2F**), CD69 (p.adj=0.015) (**Supp. Fig. 2G**), and CD25 (p.adj=0.001) (**Supp. Fig. 2H**) in the brain CD8 T cells but not in the spleen. Additionally, we further profiled these CD8 T cells using canonical makers of immunosuppression and observed an increased Lag3 (p.adj=0.036) (**Supp. Fig. 2I**) expression, but not in Tim3 (**Supp. Fig. 2J**) or Pdcd1 (**Supp. Fig. 2K**), exclusively in the brain. Lastly, we saw an increased frequency of $CD44^+$ $CD62L^-$ $CD8^+$ effector resident T cells in the brain, but not in the spleen, of BTE-treated animals (**Supp. Fig. 2L/M**).

Rechallenge of LTS mice with tumor cells demonstrated the generation of memory against glioma.

To further understand if the immunological memory in LTS mice contributes to BTE treatment, we injected parental SMA.560 glioma cells in LTS (n=5) and age-matched control mice (n=5) on the side of the brain contralateral to the original tumor implantation site. LTS mice were pooled from our two experiments using SMA.560-IL13RA2 model (**Fig. 2B, Supp. Fig.2A**). While age-matched control mice succumbed to disease within 20 days, LTS mice survived over 210 days with no sign of disease (**Fig. 3A**). Mice were subsequently sacrificed;brains were examined by histology (n=2/group) and flow cytometry (n=3/group). H&E staining revealed the presence of tumors in control mice and the absence of tumors in LTS (**Fig. 3B**). Immunohistochemical (IHC) staining of CD8 on serial tissue sections revealed a wide distribution of CD8+ T cells throughout the brain of rechallenged LTS mice (**Fig. 3C**). Quantitative analysis showed significantly more CD8+ T cells in the brains of LTS compared to controls in both the ipsilateral (p.adj=$2.22\times10-16$) and contralateral (p.adj=$4.78\times10-7$) hemispheres of the tumor injection site (**Fig. 3D**).

In our flow cytometric analysis of LTS and control brains, we observed significantly increased frequency of CD8 effector resident T cells ($CD44^+$ $CD62L^-$) (p.adj=0.0035) (**Fig. 3F**) and tissue-resident memory CD8 T cells ($CD44^+$ $CD62L^-CD103^+$) (p.adj=0.028) (**Fig. 3G)** in the brains of rechallenged LTS mice compared to control. Moreover, Ifng and TNFA expression significantly increased in CD8+ T cells of LTS compared to control (p.adj=0.093) (**Fig. 3G**). Glioma tumors are known to be highly infiltrated by $CD11B^+$ cells. We observed a significantly lower frequency of $CD11B^+$ cells in the brain of LTS mice compared to the control (**Fig. 3I**) (p.adj=0.001); this matched out histology, showing an absence of tumors in these animals.

BTE treatment results in therapeutic benefits in genetically engineered mice bearing de novo glioma tumors.

To better recapitulate human GBM, we utilized our previously reported genetically engineered mouse model (GEMM) to induce de novo gliomagenesis in adult mice [18]. This GEMM generates IL13RA2-expressing glioma tumors with loss of p53 and PTEN and overexpression of PDGFB. Histological analysis of GEMM tumors revealed key morphological characteristics of human GBM, such as pseudopalisading necrosis, microvascular proliferation, hemorrhage, heterogeneous IL13RA2, infiltration of $CD11B^+$ macrophages, and a low frequency of $CD3^+$ T cells within tumor bed (**Fig. 4A**). Treatment with BTE (n=20, MS=50.5 days) significantly extended survival in these mice compared to control (n=19, MS=41 days) (p.adj=0.0045) (**Fig. 4B**). To further understand changes within TME induced by BTE, we analyzed cells from tumor and spleen via flow cytometry 48 hours post final treatment (**Fig. 4C**). We observed no difference in regulatory T Cells in the brain between BTE and control ($CD45^+CD4^+FOXP3^+$) (p.adj=0.613) (**Fig. 4D**). Similar to experiments in orthotopic model of glioma, we saw increased expression of activation marker CD69 (p.adj=0.016) (**Fig. 4E**) in the brain but not spleen of BTE treated animals. We did not see any difference in cytotoxicity marker GZMB (p.adj=0.542) (**Fig.**

4F). We did see an increase in tissue-resident memory CD8 T cells ($CD44^+$ $CD62L^-CD103^+$) (p.adj=0.022) (**Fig. 4G**) and effector resident CD8 T cells ($CD44^+$ $CD62L^-$) (**Fig. 4H**).

Single-cell RNAseq revealed remodeling of tumor-microenvironment in *de novo* glioma tumors upon BTE treatment.

To gain insights into how BTE affects the immune microenvironment, we performed a single-cell RNA sequencing (RNA-Seq) on our GEM model following BTE treatment. We conducted two identical experiments in which tumor-bearing mice were treated with BTE or saline before the tumor microenvironment was analyzed using PIPseq™ T2 3' Single Cell RNA sequencing technology (see methods for experimental details). Like human GBM, our GEMM model contained a complex and highly heterogenous TME dominated by resident and peripheral myeloid compartments (**Fig. 5A**). Separating UMAP by treatment showed far less peripheral myeloid cells in BTE-treated animals compared to saline, observation likely due to the reduced tumor size in the BTE treated animals (**Fig. 5B**). After sub clustering and performing dimensional reduction on the T NK Cells, we identified CD4 T cells, CD8 T cells, NK cells, and regulatory T cells (**Supp. Fig 3A**), and the cells showed semi-distinct clustering differences between BTE and saline-treated animals (**Fig. 5C**). However, the relative frequency of these cells remained similar between treatment groups (**Fig. 5D**). We then performed differential gene expression analysis to understand how BTE affects the profile of CD8 T cells. Subsequent gene ontology enrichment analysis of significant DEG mapped to pathways involved in cytokine production, T cell differentiation, T cell activation, and Antigen processing and presentation (**Fig. 5E**). We then looked at specific genes key to CD8 T cell effector function and found elevated expression of genes involved in activation, cytotoxicity, and memory, and reduced expression of exhaustion genes (**Fig. 5F**).

Volumetric MRI reveals tumor-specific radiographic response and increased TME complexity upon BTE treatment.

In this study, we utilized advanced MRI techniques to gain deeper insights into the therapeutic effects of BTEs on tumor progression, therapeutic response, and microenvironmental changes in our GEM model (**Fig. 6A-D**). The representative MR 2D image of the tumor (highlighted in yellow) and the corresponding 3D rendered image generated following manual segmentation across the whole brain (Fig. 6A) depicts the reduction in whole-tumor volume we quantified following BTE treatment (**Supp. Fig. 3C**). In addition to measuring tumor size, we generated T2 parametric tumor maps of the MR 2D images to quantify tumor viability and therapy response. The intra-tumor T2 values of MR 2D images from BTE- and saline-treated animals were visualized by superimposing quantitative, color-coded parametric tumor maps; these maps were generated from multi-echo sequences using voxel-by-voxel least-squares fitting procedures (**Fig. 6B**). Further color coded (red to blue) parametric mapping of 2D MR images in multi-voxel regions revealed specific differences in radiomic-like features and patterns between BTE and

saline-treated animals (**Fig. 6C**). Derivation of quantitative tumor response and tumor viability indexes from the combination of these in vivo indexes (defined in the methods section) revealed significantly higher tumor response indexes (**Fig. 6D**) in BTE treated animals compared to saline controls.

DISCUSSION

BTEs are recognized as potent targeted T cell-based immunotherapeutics that function independently of MHC-restricted antigen recognition and exhibit strong anti-tumor activity[19, 20]. Since the FDA approval of blinatumomab in 2014 for B-cell precursor acute lymphoblastic leukemia[21], eight BTEs have been approved for use in hematopoietic malignancies. Driven by this clinical success, over 100 distinct BTEs have been evaluated in more than 250 clinical trials for applications in solid tumors[22]. However, the complex TME in solid tumors poses unique challenges for BTE therapies not encountered in liquid malignancies, and only two BTEs, Tarlatamab (small cell lung cancer)[23] and Tebentafusp (melanoma)[24], have been FDA-approved. In GBM, the highly immunosuppressive, myeloid cell-dominated TME thwarts anti-tumor immune activity[25-27]. Our group and others have demonstrated that BTEs targeting IL13RA2 and EGFRvIII elicit a powerful therapeutic effect in PDX mouse models of GBM[28, 29]. Yet, the immunodeficient mice used in these studies fail to recapitulate the hallmark immunosuppressive TME of GBM. Thus, investigating how BTEs behave in GBM models with an immune-intact TME is critical for understanding their clinically relevant therapeutic potential.

To generate the BTE suitable for studies in an immunocompetent host, we genetically fused a scFv145-2C11 recognizing murine CD3e with our anti-IL13RA2 scFv via flexible linker based on our previously validated BTE configuration[17]. *In vitro*, the resulting BTE activated and directed murine T cell-mediated killing of IL13RA2-positive murine glioma cells. *In vivo*, BTE accumulated in the brains of immunocompetent mice bearing IL13RA2-positive murine glioma after systemic injection. As such, we hypothesized that BTEs would engage host T cells and glioma cells in the brain and retain anti-tumor activity in immunocompetent models of GBM. Consistent with our hypothesis, systemic delivery of BTE resulted in target-specific T-cell activation confined to the brain tumor, with no activation observed in peripheral tissues. We demonstrated that the BTE exhibited anti-tumor activity, extending survival across all three murine GBM models, without any adverse effects. We also showed this effect was target-dependent, as no therapeutic response was seen in BTE-treated mice bearing parental glioma tumors lacking the IL13RA2. This specific on-cancer activation of T cells observed in our studies is of high importance. Using BTEs when the target is expressed in healthy tissues, even at low levels, can lead to significant damage to normal organs and neurotoxicity due to inadvertent T cell activation distant from the tumor. In fact, BTE-induced on-target, off-tumor toxicities are well-documented in solid tumors, and warrant careful consideration[30, 31]. In that respect, it is well established that IL13RA2 is a glioma-enriched antigen[32-34] and expressed in other peripheral cancers[35-40] and brain metastases[41], but not normal tissues. The specific expression of IL13RA2 in glioma but not in other cells is likely to ensure the safety of the BTE, which will be evaluated in future toxicity studies using a humanized BTE protein.

The scarcity of antigens expressed in GBM makes IL13RA2 and EGFRvIII, two antigens expressed exclusively in glioma cells and not in normal brain tissue, unique and suitable for targeted applications. Not surprisingly, these two targets are the most tested in pre-clinical and clinical settings for GBM[42]. BTE targeting EGFRvIII has been shown to significantly improve the survival of mice bearing human orthotopic glioma tumors[43], and a clinical study evaluating the molecule's safety is anticipated (NCT04903795). Our group has previously demonstrated that BTE-secreting neural stem cells (NSCs) improve the survival of mice bearing patient-derived glioma xenografts expressing IL13RA2[17]. Others also reported the therapeutic effect of different BTE configurations in GBM as a gene therapy approach[44]. However, the immense inter- and intratumoral antigen heterogeneity in GBM presents major challenges for targeted therapies, as targeting a single antigen often leads to antigen escape [45, 46]. Park and co-authors addressed this limitation using a gene therapy approach. They co-delivered two DNA-encoded BTEs targeting EGFRvIII and HER2, demonstrating superior tumor growth suppression and clearance compared to either BTE alone[9]. Others adopted a different approach to overcome GBM heterogeneity by creating multi-specific therapies, such as EGFRvIII-CAR T cells secreting anti-EGFR BTEs[10] or employing EGFR-IL13RA2-specific CAR T cells[8]; both studies showed superior efficacy compared to non-BTE secreting CAR T cells in immunocompromised mice bearing orthotopic GBM. Two clinical trials (NCT05168423, NCT05660369) evaluating the safety and feasibility of the CART-EGFR-IL13RA2 cells[11] and EGFRvIII CAR-Ts secrete EGFR-specific BTE [12] have been also launched, with initial results being reported.

The studies we conducted in immunocompetent hosts not only determined the ability of BTE to activate T cells in harsh immunosuppressive tumor environment of GBM but also discovered additional mechanisms contributing to BTE's therapeutic actions. For example, the analysis of tissues revealed a significant enrichment of tissue-resident memory (TRM) T cells in the brains of tumor-bearing mice treated with BTE across the several GBM models we tested. The increased frequency of these cells likely contributed to the complete tumor rejection in our LTS mice rechallenged with the parental glioma line lacking IL13RA2 expression. Notably, our GEM model, which recapitulates the morphology of human GBM and is characterized by a low frequency of T cells, also responded to BTE treatment and showed an increased frequency of TRM CD8 T cells. The scRNA sequencing of this GEM model revealed the CD8 T cells in the brains of BTE-treated animals displayed profiles resembling cytotoxic (CD69, GZMB, CD28, and IFNg) and memory (Sell, CD44, Itgae, CxCr3, LY6C2, CCR5) T cells with a reduced exhaustion profile (Lag3, Havcr2, Pdcd1, CC244a, and CD96) compared to control mice. TRM T cells are known to stay localized in peripheral tissues, continuously monitor their surroundings, and remain primed to rapidly respond to distress signals. These traits position TRM T cells as key contributors of anti-tumor surveillance, and there is evidence that supports response to immunotherapy is dependent on the generation of TRM T cells [47]. Evaluation of tumor tissue of both NSCLC patients[48] and melanoma patients[49] treated with anti-PD-1

checkpoint blockade therapy revealed an increase TRM CD8 T cells frequency exclusively in responders. In patients who received CAR-T cell therapy, enriched populations of TRM T cells were seen in responders to CD19- and BCMA-Specific CAR T-Cell [50]. Given the established importance of TRM T cells immunotherapeutic response and in prolonged anti-cancer immunity, our observations suggest that the TRM cells may have formed memory against glioma cells likely assisted BTE's therapeutic actions.

Studies in immunocompetent hosts provide much-needed insights into the behavior of T cells engaging therapeutics; however, there are well-documented differences between mouse and human T cells[51]. The extracellular domains of CD3E exhibit a low level of amino acid sequence conservation (47%) between humans and mice[52]. The BTE we designed and tested in this study binds murine but not human T cells[53]. It has been shown that BTEs also exhibit a relatively short plasma half-life[29]. In that respect, several modifications of BTE, such as fusion with engineered Fc or human serum albumin, offer the opportunity to significantly expand the time of the BTE in systemic circulation [54-57]. In the context of brain tumors, the balance between the circulation time and the size of the protein should be carefully investigated to ensure its sufficient penetration in GBM tissue. Thus, design of reagents suitable for both human and mouse studies, along with modifications that enhance penetration into brain tumors and improve plasma stability, is essential to overcome the limitations of pre-clinical testing for the clinical translation of BTEs.

In conclusion, our study demonstrates the survival benefits of BTEs in several orthotopic and GEM models of GBM, along with specific immune engagement with the target, induction of immunological memory, and modulation of the tumor microenvironment. This provides strong evidence of BTE-induced responses and the engagement of the host immune system, reinforcing BTE's mechanism of action. These findings also encourage further investigation into other brain and peripheral cancers expressing IL13RA2. While combating GBM remains our primary focus, translating this immunotherapeutic strategy may offer therapeutic benefits in other solid tumors, warranting further exploration of its full potential.

DISCLOSURE OF POTENTIAL CONFLICTS OF INTEREST

IVB is the inventor of a patent on the single-chain antibody against IL13RA2, which was utilized in the current study to generate IL13RA2 BTE.

ACKNOWLEDGMENTS

This study was partly supported by the following grants: NINDS R33 NS101150, R01 NS106379, and R01 NS122395 (IVB). The authors thank the Mouse Histology and Phenotyping

Laboratory and the Small Animal Imaging Cores, supported by National Cancer Institute Grant P30-CA060553, awarded to the Robert H. Lurie Comprehensive Cancer Center for their excellent service.

AUTHOR CONTRIBUTIONS.

IVB conceived the study and provided funding; MZ, JTD, IVB designed experiments; MZ, JTD, DP, and RNL performed experiments; DH and BZ provided expertise on GEM and Nur77 mouse models; MZ, JTD, DP, LL, C.L-C, JM, and IVB performed data analysis; MZ, JTD, DP, and IVB co-wrote the manuscript. MZ and JTD contributed equally to this work.All authors met the criteria for authorship and approved the final manuscript for publication.

LEGENDS TO FIGURES.

Figure 1. Generation and Functional Characterization of CD3xIL13RA2 BTE. (*A*) Schematic representation of BTE. BTE consisted of the scFv targeting murine CD3E specific, derived from 2C11-145, and the scFv targeting IL13RA2, derived from clone47, fused together via a flexible GlyS (Gly4Ser) linker. Negative control BTE (NC-BTE) differed from BTE in the VH domain of IL13RA2-scFv, which was swapped with the VH domain of scFv p588 of the non-specific MOPC21 antibody. (*B*) A western blot of affinity-purified BTE was detected using anti-His HRP conjugated antibodies, and a specific single band ~was observed at 55 kDa. (*C*) ELISA assay of affinity purified BTE and NC-BTE demonstrating dose-dependent and specific binding of BTE, but not NC-BTE, to recombinant IL13RA2, but not to IL13RA1 (*D*) Chromium-51 (Cr51) release assay of murine T cells and murine glioma cells treated with BTE (red), NC-BTE (white), or Dynabeads™ Mouse T-Activator CD3/CD28 (grey) showing BTE, but not NC-BTE, induced dose-dependent killing of IL13Rα2-expressing SMA560 and GL261 murine glioma cells (Effector-to-target [E : T] ratio = 20:1; Incubation time = 24 hr; n=3/group). (*E*) Flow cytometric analysis of murine T cells co-cultured with IL13Rα2-expressing SMA560, GL261, and CT2A murine glioma cells showing BTE, but not NC-BTE induced robust expression T cell activation markers CD69 and CD25 (Effector-to-target [E: T] ratio = 20:1; Incubation time = 24 hr; n=3/group). One-way ANOVA followed by Tukey's Honest Significant Difference (HSD) test for pairwise comparisons)

Figure 2. BTE Enhances Survival and Modulates Tumor Microenvironment of Mice Bearing IL13RA2-expressing SMA560 glioma. (*A*) Dynamic live fluorescent imaging of AF647-labeled BTE showing penetration and persistence in the brains of GL261-IL13RA2 tumor-bearing mice (Fluorescent signal measured as radiance [p/s/cm2/sr]; Image acquisition time = 3, 6, 24, 48, and 72 hrs post AF647-BTE injection; n=3). (*B*) Kaplan–Meier survival curve of SMA.560-IL13RA2 tumor-bearing mice treated with either BTE (200 µg/animal) (red), NC-BTE (200 µg/animal) (blue), or saline (black). Wald test from Cox proportional hazards regression analysis (*C*) Experimental setup used in flow cytometric analysis of the brains of SMA.560-IL13RA2 tumor-bearing mice following treatment with either BTE or NC-BTE (n=5/group). Flow cytometric analysis revealed (*D*) no change in CD4 helper t cell (CD45+ CD4+), (*E*) increase in regulatory T cell (CD45+ CD4+ FOXP3+), (*F*) increase in CD8 T cell (CD45+ CD8+), (*G*) increase in memory-like CD8 T cell (CD45+CD8+CD127HiKLRG1−), (*H*) no change in short-lived

memory CD8 T cells (CD45+ CD8+ CD127Hi KLRG1+), (*I*) increase in tissue-resident memory CD8 T cells (CD45+ CD8+ CD127Hi KLRG1− CD103+), (*J*) increase in monocytic MDSC (mo.MDSC) (CD45+ CD11B+ CD11C−LY6G− LY6C+), (*K*) no change in polymorphonuclear MDSC (PMN.MDSC) (CD45+ CD11B+ CD11C− LY6G+ LY6C+), (*L*) no change in dendritic cells (CD45+ CD11B+ CD11C+). One-way ANOVA followed by Tukey's Honest Significant Difference (HSD) test for pairwise comparisons).

Figure 3. Rechallenge of LTS mice with tumor cells demonstrated the generation of memory against glioma. (*A*) Kaplan–Meier survival curve of long-term surviving (LTS) (red) and age-matched control (black) following injection of parental SMA.560 murine glioma cell line into the brain hemisphere contralateral to the primary tumor implantation site. Animals were followed for survival, and statistical significance was tested via the Wald test from Cox proportional hazards regression analysis. (*B*) The mice of LTS (210 days post-secondary injection) and age-matched control (at endpoint) were sacrificed and stained using H&E to check for the presence of tumors in the ipsilateral and contralateral hemispheres of the primary injection site. Scale bar represents 2.5 mm. (*C, D*) Serial sections of the same brains stained for infiltrating CD8+ T cells. (*C*) Representative image of one LTS-ipsilateral section with magnified images in the cerebrum (arrowheads) and the cerebellum (arrowheads). The scale bar represents 2.5 mm for the H&E image and 100 µm for magnified anti-CD8 IHC. (*D*) Quantitative analysis of CD8+ T cells in the ipsilateral and contralateral hemispheres of the brain of LTS, age-matched control, and non-tumor bearing mice. One-way ANOVA. (*E-H*) Flow cytometric analysis of freshly dissected brains of LTS (red) and age-matched control (white); n=3/group. (*E*) A representative contour plot shows an increased frequency of CD8 resident T cells (CD44+ CD62L-) in the brains of LTS (left) compared to the control (right). Quantified frequency of (F) tissue-resident memory CD8 T cells (CD8+ CD44+ CD62L- CD103+), (G) inflammatory cytokine producing CD8 T cell (CD8+ TNFα +IFNγ +), and (H) total population of myeloid cells (CD45+ CD11B+). Differences among multiple groups were evaluated using one-way or two-way ANOVA with Tukey's Honest Significant Difference (HSD) test.

Figure 4. BTE treatment results in therapeutic benefits in genetically engineered mice bearing de novo glioma tumors. (*A*) Histopathological analysis of RCAS-P53fl/fl-PTENfl/fl-IL13RA2 GEMM glioma model with high magnification images showing morphological characteristics similar to human GBM. H&E (top-left) shows areas of pseudopalisading necrosis (i), microvascular proliferation (ii), and hyperplasia (iii). IHC staining revealed many infiltrating CD11B+ macrophages (top-right), scarce infiltrating CD3+ T cells (bottom-right), and heterogeneous IL13RA2 expression (bottom-left) within the tumor bed. (*B*) Kaplan–Meier survival curve of de novo GEMM glioma model treated with BTE (red) (n=20) or saline (black) (n=19). Animals were followed for survival, and statistical significance was tested via Wald test from Cox proportional hazards regression analysis. (*C*) An experimental setup was used in flow cytometric analysis of the brains and spleens of the GEMM glioma model following treatment with either BTE or saline (n=5/group). Flow cytometric analysis revealed (*D*) no change in regulatory T cell (CD45+ CD4+ FOXP3+) and brain-specific increases in (*E*) activated CD8 T cell (CD45+ CD8+ CD69+), (*F*) cytotoxic CD8 T cell (CD45+ CD8+ CD69+), (*H*) resident CD8 T cells (CD45+ CD8+ CD44+ CD62L-), and (*G*) tissue-resident memory CD8 T cells (CD45+ CD8+ CD44+ CD62L- CD103+).

Figure 5. Single-cell RNAseq revealed remodeling of tumor-microenvironment in de novo glioma tumors upon BTE treatment. (*A*) UMAP visualization of cell clusters identified through CCA integration of single-cell RNA sequencing data from cells isolated from the brains of our de novo GEMM glioma model treated with BTE or saline. The dataset includes 64,124 cells from four samples (two BTE-treated and two saline-treated), with each sample comprising cells pooled from five mice. Cells were

enriched for CD45-positive populations at a CD45+:CD45- ratio of 8:2. (*B*) Identical UMAP ordered by treatment. (*C*) UMAP visualization of T and NK cell subclustering following CCA integration, displayed for the saline treatment group (top) and the BTE treatment group (bottom). Subclusters include CD8 T cells (red), CD4 T cells (blue), regulatory T cells (green), γδ T cells (brown), and NK cells (purple), highlighting differences between the treatment groups. (*D*) Relative cell frequency of CD8 T cells (blue), CD4 T cells (red), regulatory T cells (green), γδ T cells (brown), and NK cells (purple) separated by sample treatment. (*E*) Gene ontology analysis of differentially expressed genes (DEGs) in CD8 T cells between BTE and Saline treated samples. (*F*) Heatmap of DEGs in CD8 T cell cluster across all samples related to activation-cytotoxicity, CD8 T cell memory, and exhaustion.

Figure. 6: Magnetic Resonance Imaging demonstrates responses of de novo tumors to BTE in GEM model. (*A*) depicts a representative set of two MRI gray-scale anatomical brain sections for a saline control (left) and BTE-treated (right) mouse. Whole-tumor 3D delineation was done to extract tumor size and to enable rendered 3D visualization of the overall tumor size. (*B*) A representative set of two quantitative T2 parametric colored maps for a saline control and BTE-treated mouse is overlayed on a corresponding anatomical gray-scale image. (*C*) Comparative clustered T2 parametric image of each tumor (control saline on the left and BTE-treated on the right) with different colors depicting intratumor regions with different T2 values (BLUE/CYAN low values and YELLOW/RED high values). An H&E stain of a representative section for each mouse was selected to match the exact location of the MR-derived image as closely as possible (using anatomical features). The clustered intra-tumor regions were then used to extract volumetric quantities for each T2 range, with the driving hypothesis (from our work and existing literature) that an overall decrease in T2 tumor values can be associated with therapeutic response. (*D*) box-chart plot of each mouse's Tumor Response Index values, which agree with survival analysis, flow cytometry, and RNAseq data.

LEGENDS TO SUPPLEMENTAL FIGURES.

Supplementary Figure 1. Generation and Functional Characterization of CD3xIL13RA2 BTE. (*A*) Representative Incucyte-generated images of murine T cells isolated from NOD.Nr4a1GFP/Cre mice cocultured with GL261-Il13RA2 glioma cells at 2 hours and 17 hours post-treatment with NC-BTE (left), BTE (middle), and Dynabeads™ Mouse T-Activator CD3/CD28 (right). Briefly, Nr4a1 is a transcription factor that is downstream of TCR signaling. NOD.Nr4a1GFP/Cre mice contain a cre recombinase/green fluorescent fusion protein driven by the Nr4a1 (e.g., Nur77) promoter. Thus, NOD.Nr4a1GFP/Cre T cells began to express GFP following activation and were used as reporter assays to visualize BTE-mediated T cell activation. (*B*) Quantification of mean fluorescent intensities from Incucyte NOD.Nr4a1GFP/Cre T cell activation experiment. (*C*) Cr51 release assay of Chromium-51 (Cr51) release assay of either parental (blue) or IL13RA2 modified (brown) SMA560 (left) and GL261(right) murine glioma cells co-cultured with murine T cells and treated with varying doses of BTE or Dynabeads™ Mouse T-Activator CD3/CD28 (Activated) showing BTE mediated killing is IL13RA2 antigen-dependent (Effector-to-target [E: T] ratio = 20:1; Incubation time = 24 hr; n=3/group).

Supplementary Figure 2. BTE Enhances Survival and Modulates Tumor Microenvironment of Mice Bearing IL13RA2-expressing murine glioma. (*A*) Kaplan–Meier survival curve of SMA.560-IL13RA2 tumor-bearing mice treated with BTE at 200 µg/animal (red), BTE (50 µg/animal) (green), or saline (black). Wald test from Cox proportional hazards regression analysis. (*B*) Kaplan–Meier survival curve of parental SMA.560 tumor-bearing mice treated with BTE at 200 µg/animal (red), NC-BTE (200 µg/animal) (blue), or saline (black). Wald test from Cox

proportional hazards regression analysis (*C*) Kaplan–Meier survival curve of CT2A-IL13RA2 tumor-bearing mice treated with BTE at 200 µg/animal (red), NC-BTE (200 µg/animal) (blue), or saline (black). Wald test from Cox proportional hazards regression analysis. (*D*) An experimental setup was used in flow cytometric analysis of the brains of SMA.560-IL13RA2 tumor-bearing mice following treatment with either BTE or NC-BTE (n=5/group). Flow cytometric analysis revealed (*E*) increase in regulatory T cell (CD45+CD4+FOXP3+), (*F*) increase in cytotoxic CD8 T cell (CD45+CD8+GZMB+), (*G*) increase in activated CD69 expressing (CD45+CD8+CD69+) and (*H*) activated CD25 expressing CD8 T cells (CD45+CD8+CD25+), (*I*) increase in Lag3 expressing CD8 T cells (CD45+CD8+ Lag3+), (*J*) no change in Tim3 expressing CD8 T cells (CD45+ CD8+ Tim3+), (*K*) no change in Pdcd1 expressing CD8 T cells (CD45+ CD8+ Pdcd1+), and (L/M) increase in effector CD8 T cells (CD45+ CD11B+ CD11C−LY6G− LY6C+). One-way ANOVA followed by Tukey's Honest Significant Difference (HSD) test for pairwise comparisons).

Supplementary Figure 3. Identifying T and NK cell subcluster markers from single-cell RNA seq and tumor volume from MRI. (*A*) Relative expression of CD3e, CD8a, CD4, FOXP3, Trdc, Trgc1, and Klrb1c used as identifying markers of T and NK cell subcluster of single cell RNA seq. (*B*) Box plot of tumor volume from MRI of BTE (n=3) and Saline (n=3) treated animals. (*C*) Histogram of voxel T2 MRI images separated by BTE and Saline treatment groups.

REFERENCES

1. Alexander, B.M. and T.F. Cloughesy, *Adult glioblastoma.* Journal of Clinical Oncology, 2017. **35**(21): p. 2402-2409.
2. Stupp, R., et al., *Radiotherapy plus concomitant and adjuvant temozolomide for glioblastoma.* New England journal of medicine, 2005. **352**(10): p. 987-996.
3. Bi, W.L. and R. Beroukhim, *Beating the odds: extreme long-term survival with glioblastoma*. 2014, Society for Neuro-Oncology. p. 1159-1160.
4. Stupp, R., et al., *Effect of tumor-treating fields plus maintenance temozolomide vs maintenance temozolomide alone on survival in patients with glioblastoma: a randomized clinical trial.* Jama, 2017. **318**(23): p. 2306-2316.
5. Alsajjan, R. and W.P. Mason, *Bispecific T-cell engagers and chimeric antigen receptor T-cell therapies in glioblastoma: an update.* Current Oncology, 2023. **30**(9): p. 8501-8549.
6. Gedeon, P.C., et al., *GLP toxicology study of a fully-human T cell redirecting CD3: EGFRvIII binding immunotherapeutic bispecific antibody.* Plos one, 2020. **15**(7): p. e0236374.
7. Sonabend, A.M., et al., *Repeated blood-brain barrier opening with an implantable ultrasound device for delivery of albumin-bound paclitaxel in patients with recurrent glioblastoma: a phase 1 trial.* Lancet Oncol, 2023. **24**(5): p. 509-522.
8. Yin, Y., et al., *Locally secreted BiTEs complement CAR T cells by enhancing killing of antigen heterogeneous solid tumors.* Mol Ther, 2022. **30**(7): p. 2537-2553.
9. Park, D.H., et al., *Multivalent in vivo delivery of DNA-encoded bispecific T cell engagers effectively controls heterogeneous GBM tumors and mitigates immune escape.* Molecular Therapy-Oncolytics, 2023. **28**: p. 249-263.
10. Choi, B.D., et al., *CAR-T cells secreting BiTEs circumvent antigen escape without detectable toxicity.* Nature biotechnology, 2019. **37**(9): p. 1049-1058.
11. Bagley, S.J., et al., *Intrathecal bivalent CAR T cells targeting EGFR and IL13Rα2 in recurrent glioblastoma: phase 1 trial interim results.* Nature Medicine, 2024. **30**(5): p. 1320-1329.
12. Choi, B.D., et al., *Intraventricular CARv3-TEAM-E T cells in recurrent glioblastoma.* New England Journal of Medicine, 2024. **390**(14): p. 1290-1298.
13. Pituch, K.C., et al., *Adoptive Transfer of IL13Ralpha2-Specific Chimeric Antigen Receptor T Cells Creates a Pro-inflammatory Environment in Glioblastoma.* Mol Ther, 2018. **26**(4): p. 986-995.
14. Leo, O., et al., *Identification of a monoclonal antibody specific for a murine T3 polypeptide.* Proc Natl Acad Sci U S A, 1987. **84**(5): p. 1374-8.
15. Balyasnikova, I.V., et al., *Characterization and immunotherapeutic implications for a novel antibody targeting interleukin (IL)-13 receptor α2.* J Biol Chem, 2012. **287**(36): p. 30215-27.
16. Kim, J.W., et al., *A novel single-chain antibody redirects adenovirus to IL13Rα2-expressing brain tumors.* Sci Rep, 2015. **5**: p. 18133.
17. Pituch, K.C., et al., *Neural stem cells secreting bispecific T cell engager to induce selective antiglioma activity.* Proc Natl Acad Sci U S A, 2021. **118**(9).
18. Seblani, M., et al., *A New Mouse Model of Diffuse Midline Glioma to Test Targeted Immunotherapies.* bioRxiv, 2021: p. 2021.10.15.464284.
19. Dreier, T., et al., *Extremely potent, rapid and costimulation-independent cytotoxic T-cell response against lymphoma cells catalyzed by a single-chain bispecific antibody.* International journal of cancer, 2002. **100**(6): p. 690-697.

20. Offner, S., et al., *Induction of regular cytolytic T cell synapses by bispecific single-chain antibody constructs on MHC class I-negative tumor cells.* Molecular immunology, 2006. **43**(6): p. 763-771.
21. Przepiorka, D., et al., *FDA approval: blinatumomab.* Clinical Cancer Research, 2015. **21**(18): p. 4035-4039.
22. Liu, J. and J. Zhu, *Progresses of T-cell-engaging bispecific antibodies in treatment of solid tumors.* International Immunopharmacology, 2024. **138**: p. 112609.
23. Dhillon, S., *Tarlatamab: First Approval.* Drugs, 2024: p. 1-9.
24. Dhillon, S., *Tebentafusp: first approval.* Drugs, 2022. **82**(6): p. 703-710.
25. Quail, D.F. and J.A. Joyce, *The microenvironmental landscape of brain tumors.* Cancer cell, 2017. **31**(3): p. 326-341.
26. Bowman, R.L., et al., *Macrophage ontogeny underlies differences in tumor-specific education in brain malignancies.* Cell reports, 2016. **17**(9): p. 2445-2459.
27. Wang, G., et al., *Tumor-associated microglia and macrophages in glioblastoma: From basic insights to therapeutic opportunities.* Frontiers in immunology, 2022. **13**: p. 964898.
28. Pituch, K.C., et al., *Neural stem cells secreting bispecific T cell engager to induce selective antiglioma activity.* Proceedings of the National Academy of Sciences, 2021. **118**(9): p. e2015800118.
29. Schaller, T.H., et al., *Pharmacokinetic analysis of a novel human EGFRvIII: CD3 bispecific antibody in plasma and whole blood using a high-resolution targeted mass spectrometry approach.* Journal of proteome research, 2019. **18**(8): p. 3032-3041.
30. van de Donk, N.W. and S. Zweegman, *T-cell-engaging bispecific antibodies in cancer.* The Lancet, 2023. **402**(10396): p. 142-158.
31. Cattaruzza, F., et al., *Precision-activated T-cell engagers targeting HER2 or EGFR and CD3 mitigate on-target, off-tumor toxicity for immunotherapy in solid tumors.* Nature Cancer, 2023. **4**(4): p. 485-501.
32. Zeng, J., et al., *IL13RA2 is overexpressed in malignant gliomas and related to clinical outcome of patients.* American journal of translational research, 2020. **12**(8): p. 4702.
33. Joshi, B.H., G.E. Plautz, and R.K. Puri, *Interleukin-13 receptor α chain: a novel tumor-associated transmembrane protein in primary explants of human malignant gliomas.* Cancer research, 2000. **60**(5): p. 1168-1172.
34. Bhardwaj, R., et al., *Identification of a novel role of IL-13Rα2 in human Glioblastoma multiforme: interleukin-13 mediates signal transduction through AP-1 pathway.* Journal of Translational Medicine, 2018. **16**: p. 1-13.
35. Kawakami, K., P. Leland, and R.K. Puri, *Structure, function, and targeting of interleukin 4 receptors on human head and neck cancer cells.* Cancer research, 2000. **60**(11): p. 2981-2987.
36. Kawakami, M., et al., *Interleukin-13 receptor α2 chain in human head and neck cancer serves as a unique diagnostic marker.* Clinical cancer research, 2003. **9**(17): p. 6381-6388.
37. Bartolomé, R.A., et al., *Protein tyrosine phosphatase-1B inhibition disrupts IL13Rα2-promoted invasion and metastasis in cancer cells.* Cancers, 2020. **12**(2): p. 500.
38. Fujisawa, T., et al., *A novel role of interleukin-13 receptor α2 in pancreatic cancer invasion and metastasis.* Cancer research, 2009. **69**(22): p. 8678-8685.
39. Okamoto, H., et al., *Interleukin-13 receptor α2 is a novel marker and potential therapeutic target for human melanoma.* Scientific reports, 2019. **9**(1): p. 1281.
40. Papageorgis, P., et al., *Targeting IL13Ralpha2 activates STAT6-TP63 pathway to suppress breast cancer lung metastasis.* Breast Cancer Research, 2015. **17**: p. 1-15.
41. Márquez-Ortiz, R.A., et al., *IL13Rα2 promotes proliferation and outgrowth of breast cancer brain metastases.* Clinical Cancer Research, 2021. **27**(22): p. 6209-6221.

42. Shikalov, A., I. Koman, and N.M. Kogan, *Targeted glioma therapy—clinical trials and future directions.* Pharmaceutics, 2024. **16**(1): p. 100.
43. Gedeon, P.C., et al., *A Rationally Designed Fully Human EGFRvIII:CD3-Targeted Bispecific Antibody Redirects Human T Cells to Treat Patient-derived Intracerebral Malignant Glioma.* Clin Cancer Res, 2018. **24**(15): p. 3611-3631.
44. Bhojnagarwala, P.S., et al., *In vivo DNA-launched bispecific T cell engager targeting IL-13Ralpha2 controls tumor growth in an animal model of glioblastoma multiforme.* Mol Ther Oncolytics, 2022. **26**: p. 289-301.
45. Brown, C.E., et al., *Regression of glioblastoma after chimeric antigen receptor T-cell therapy.* New England Journal of Medicine, 2016. **375**(26): p. 2561-2569.
46. O'Rourke, D.M., et al., *A single dose of peripherally infused EGFRvIII-directed CAR T cells mediates antigen loss and induces adaptive resistance in patients with recurrent glioblastoma.* Science translational medicine, 2017. **9**(399): p. eaaa0984.
47. Okła, K., D.L. Farber, and W. Zou, *Immune Memory Focus: Tissue-resident memory T cells in tumor immunity and immunotherapy.* The Journal of experimental medicine, 2021. **218**(4).
48. Corgnac, S., et al., *CD103+ CD8+ TRM cells accumulate in tumors of anti-PD-1-responder lung cancer patients and are tumor-reactive lymphocytes enriched with Tc17.* Cell Reports Medicine, 2020. **1**(7).
49. Edwards, J., et al., *CD103+ tumor-resident CD8+ T cells are associated with improved survival in immunotherapy-naïve melanoma patients and expand significantly during anti–PD-1 treatment.* Clinical Cancer Research, 2018. **24**(13): p. 3036-3045.
50. Wang, M., et al., *Identification and validation of predictive biomarkers to CD19-and BCMA-specific CAR T-cell responses in CAR T-cell precursors.* Blood, 2019. **134**: p. 622.
51. Mestas, J. and C.C. Hughes, *Of mice and not men: differences between mouse and human immunology.* The Journal of Immunology, 2004. **172**(5): p. 2731-2738.
52. Ueda, O., et al., *Entire CD3ε, δ, and γ humanized mouse to evaluate human CD3–mediated therapeutics.* Scientific reports, 2017. **7**(1): p. 45839.
53. Miescher, G.C., M. Schreyer, and H.R. MacDonald, *Production and characterization of a rat monoclonal antibody against the murine CD3 molecular complex.* Immunology letters, 1989. **23**(2): p. 113-118.
54. Suurs, F.V., et al., *Mesothelin/CD3 Half-Life–Extended Bispecific T-Cell Engager Molecule Shows Specific Tumor Uptake and Distributes to Mesothelin and CD3-Expressing Tissues.* Journal of Nuclear Medicine, 2021. **62**(12): p. 1797-1804.
55. Lorenczewski, G., et al., *Generation of a half-life extended anti-CD19 BiTE® antibody construct compatible with once-weekly dosing for treatment of CD19-positive malignancies.* Blood, 2017. **130**: p. 2815.
56. Arvedson, T.L., et al., *Generation of half-life extended anti-CD33 BiTE® antibody constructs compatible with once-weekly dosing.* Cancer Research, 2017. **77**(13_Supplement): p. 55-55.
57. Mandrup, O.A., et al., *Programmable half-life and anti-tumour effects of bispecific T-cell engager-albumin fusions with tuned FcRn affinity.* Communications biology, 2021. **4**(1): p. 310.

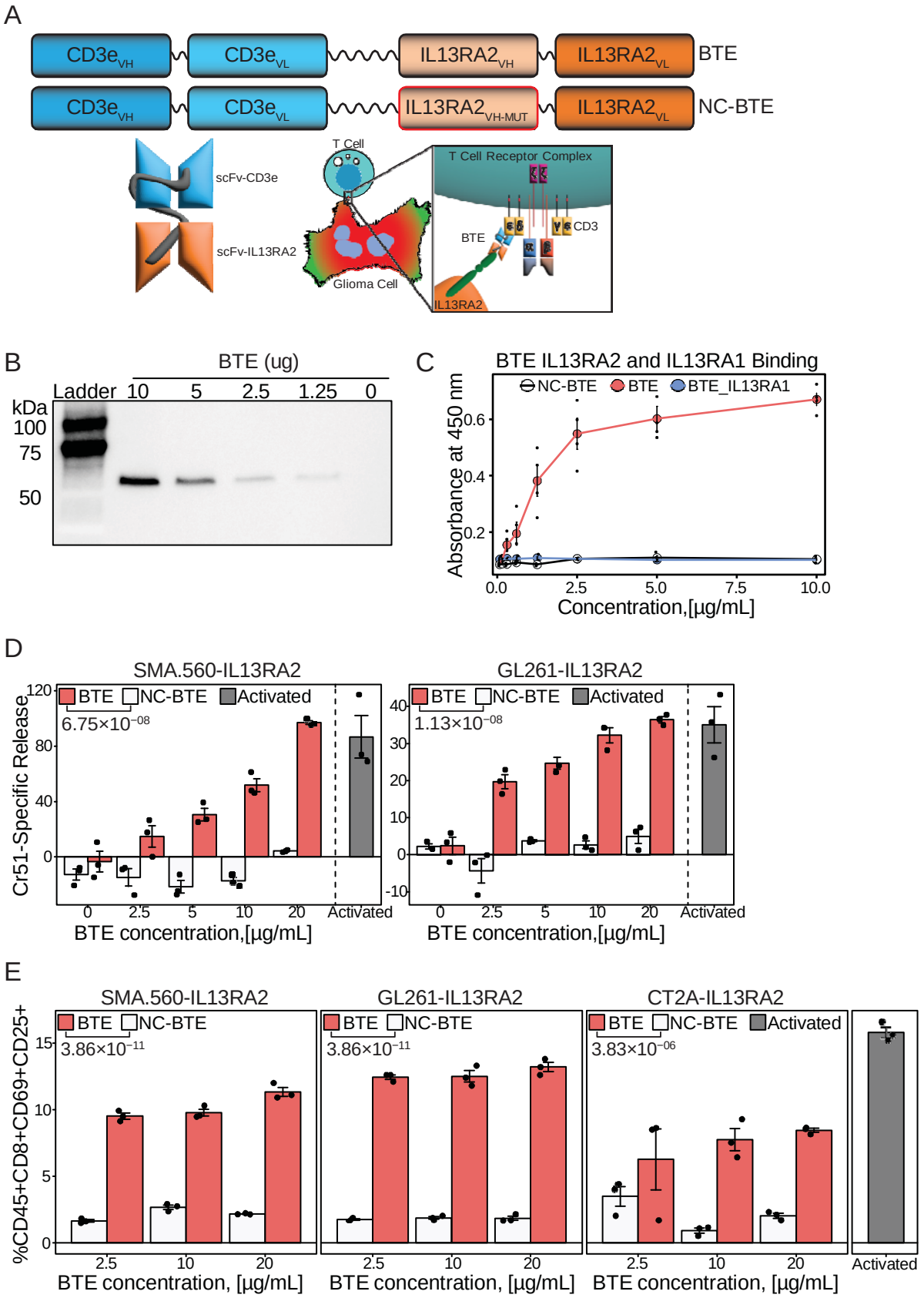
A
CD3e$_{VH}$
CD3e$_{VL}$
IL13RA2$_{VH}$
IL13RA2$_{VL}$
BTE
IL13RA2$_{VH-MUT}$
NC-BTE
scFv-CD3e
scFv-IL13RA2
T Cell
Glioma Cell
T Cell Receptor Complex
CD3
IL13RA2
B
BTE (ug)
Ladder
10
5
2.5
1.25
0
kDa
100
75
50
C
BTE IL13RA2 and IL13RA1 Binding
NC-BTE
BTE
BTE_IL13RA1
Absorbance at 450 nm
Concentration,[µg/mL]
D
SMA.560-IL13RA2
GL261-IL13RA2
BTE
NC-BTE
Activated
6.75×10^{-08}
1.13×10^{-08}
Cr51-Specific Release
BTE concentration,[µg/mL]
E
SMA.560-IL13RA2
GL261-IL13RA2
CT2A-IL13RA2
3.86×10^{-11}
3.86×10^{-11}
3.83×10^{-06}
%CD45+CD8+CD69+CD25+
BTE concentration, [µg/mL]

Figure 1

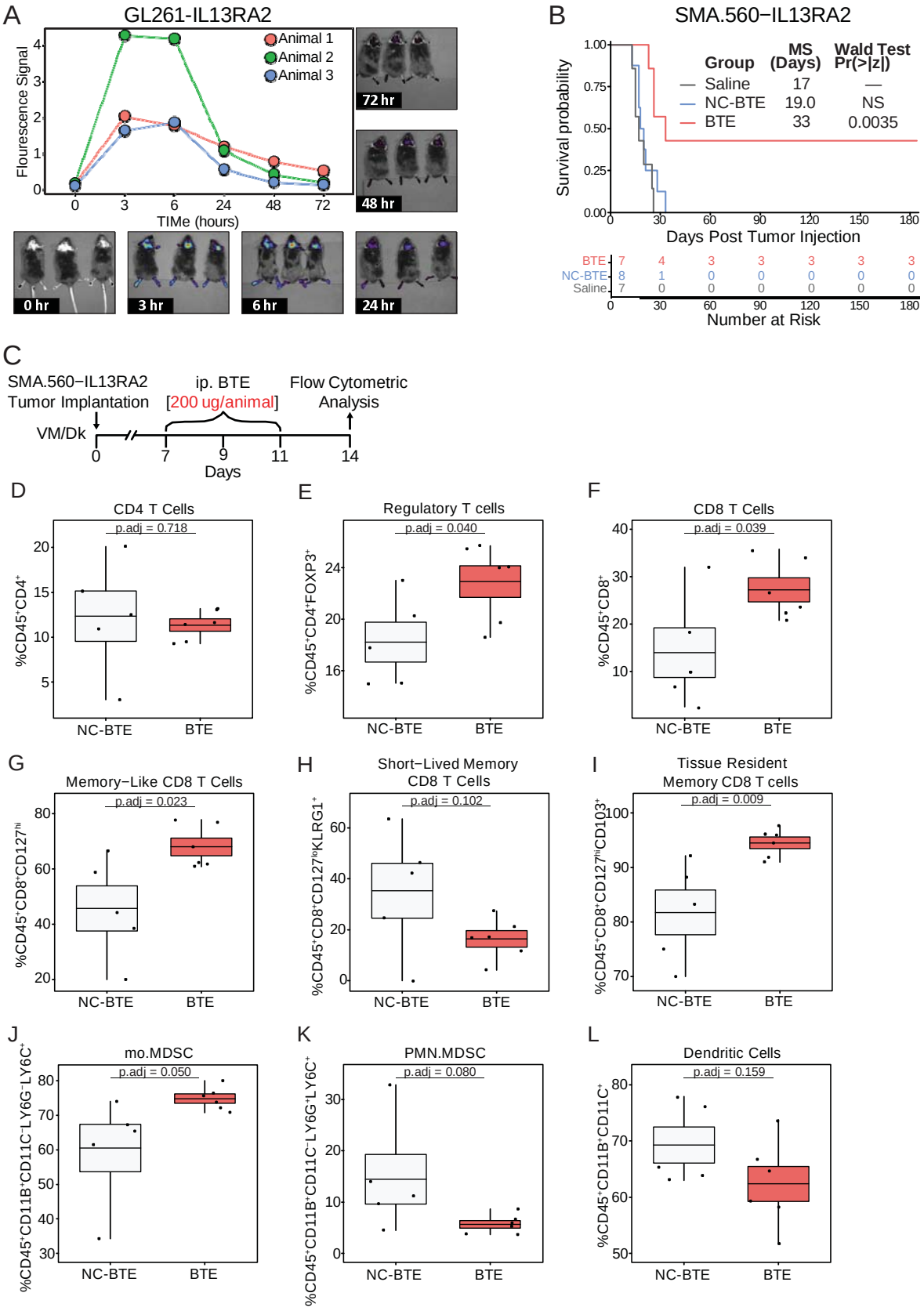
A
GL261-IL13RA2
Flourescence Signal
Animal 1
Animal 2
Animal 3
TIMe (hours)
72 hr
48 hr
0 hr
3 hr
6 hr
24 hr
B
SMA.560−IL13RA2
Survival probability
Group
MS (Days)
Wald Test Pr(>|z|)
Saline 17 —
NC-BTE 19.0 NS
BTE 33 0.0035
Days Post Tumor Injection
Number at Risk
C
SMA.560−IL13RA2 Tumor Implantation
ip. BTE [200 ug/animal]
Flow Cytometric Analysis
VM/Dk
Days
D
CD4 T Cells
p.adj = 0.718
%CD45+CD4+
E
Regulatory T cells
p.adj = 0.040
%CD45+CD4+FOXP3+
F
CD8 T Cells
p.adj = 0.039
%CD45+CD8+
G
Memory−Like CD8 T Cells
p.adj = 0.023
%CD45+CD8+CD127hi
H
Short−Lived Memory CD8 T Cells
p.adj = 0.102
%CD45+CD8+CD127loKLRG1+
I
Tissue Resident Memory CD8 T cells
p.adj = 0.009
%CD45+CD8+CD127hiCD103+
J
mo.MDSC
p.adj = 0.050
%CD45+CD11B+CD11C-LY6G-LY6C+
K
PMN.MDSC
p.adj = 0.080
%CD45+CD11B+CD11C-LY6G+LY6C+
L
Dendritic Cells
p.adj = 0.159
%CD45+CD11B+CD11C+
NC-BTE
BTE

Figure 2

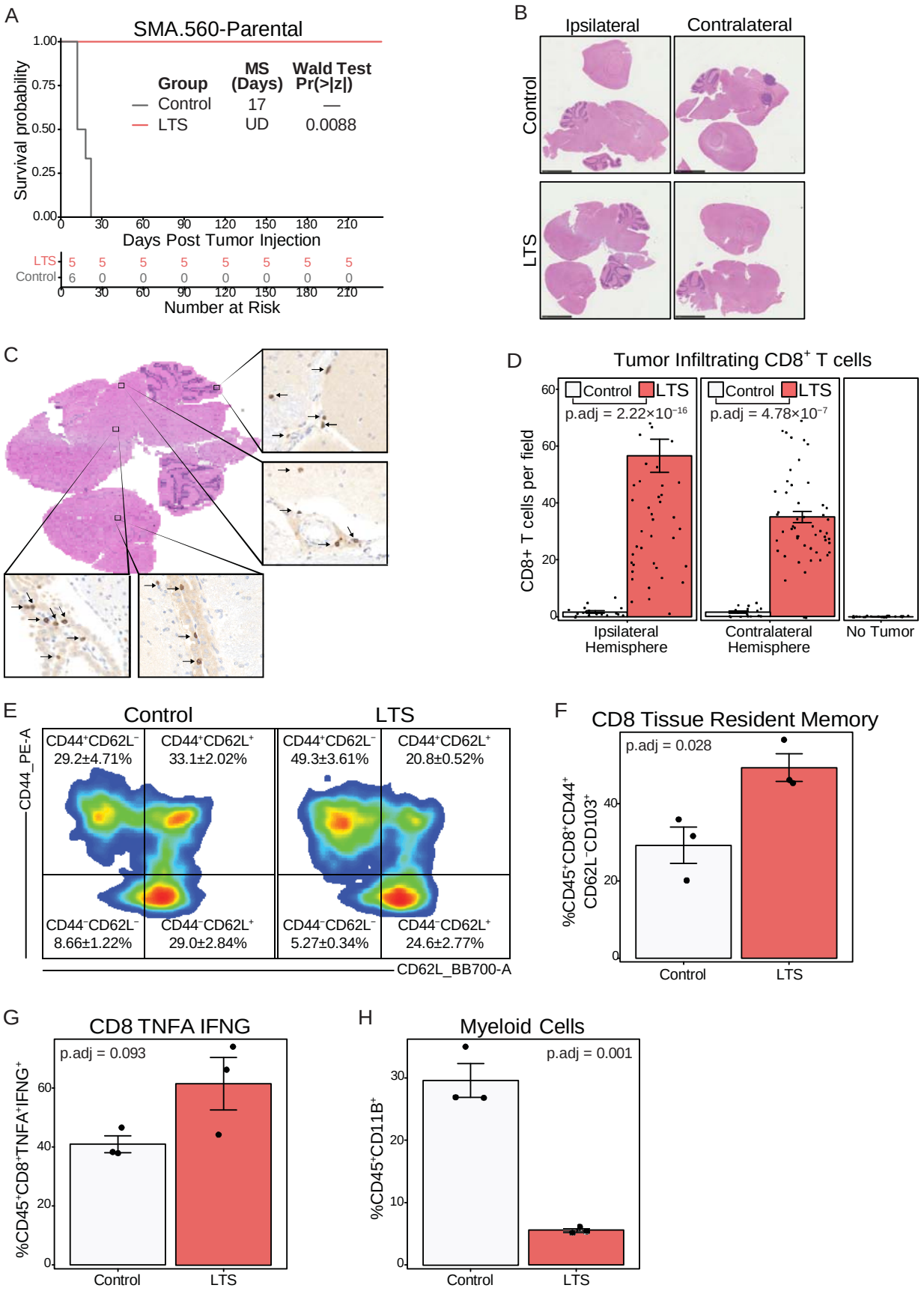
A
SMA.560-Parental
Survival probability
1.00
0.75
0.50
0.25
0.00
Group
MS (Days)
Wald Test Pr(>|z|)
Control 17 —
LTS UD 0.0088
0 30 60 90 120 150 180 210
Days Post Tumor Injection
LTS 5 5 5 5 5 5 5 5
Control 6 0 0 0 0 0 0 0
Number at Risk
B
Ipsilateral
Contralateral
Control
LTS
C
D
Tumor Infiltrating CD8+ T cells
Control LTS
p.adj = 2.22×10−16
p.adj = 4.78×10−7
CD8+ T cells per field
Ipsilateral Hemisphere
Contralateral Hemisphere
No Tumor
E
Control
LTS
CD44_PE-A
CD44+CD62L− 29.2±4.71%
CD44+CD62L+ 33.1±2.02%
CD44+CD62L− 49.3±3.61%
CD44+CD62L+ 20.8±0.52%
CD44−CD62L− 8.66±1.22%
CD44−CD62L+ 29.0±2.84%
CD44−CD62L− 5.27±0.34%
CD44−CD62L+ 24.6±2.77%
CD62L_BB700-A
F
CD8 Tissue Resident Memory
p.adj = 0.028
%CD45+CD8+CD44+ CD62L−CD103+
Control
LTS
G
CD8 TNFA IFNG
p.adj = 0.093
%CD45+CD8+TNFA+IFNG+
Control
LTS
H
Myeloid Cells
p.adj = 0.001
%CD45+CD11B+
Control
LTS

Figure 3

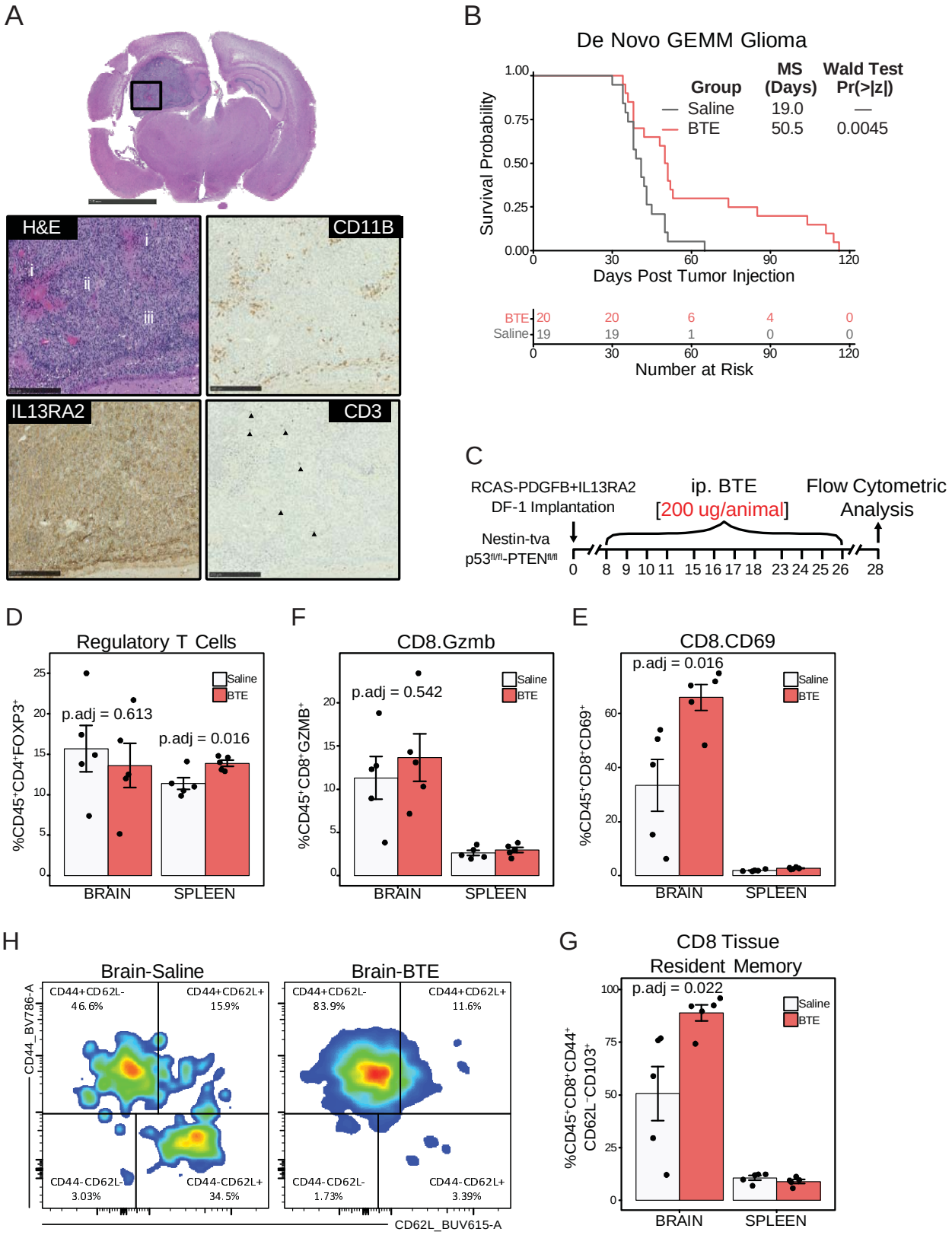
A
H&E
CD11B
IL13RA2
CD3
i
ii
iii
B
De Novo GEMM Glioma
Group
MS (Days)
Wald Test Pr(>|z|)
Saline 19.0 —
BTE 50.5 0.0045
Survival Probability
Days Post Tumor Injection
BTE 20 20 6 4 0
Saline 19 19 1 0 0
Number at Risk
C
RCAS-PDGFB+IL13RA2
DF-1 Implantation
Nestin-tva
p53fl/fl-PTENfl/fl
ip. BTE
[200 ug/animal]
Flow Cytometric Analysis
0 8 9 10 11 15 16 17 18 23 24 25 26 28
D
Regulatory T Cells
%CD45+CD4+FOXP3+
p.adj = 0.613
p.adj = 0.016
Saline
BTE
BRAIN
SPLEEN
F
CD8.Gzmb
%CD45+CD8+GZMB+
p.adj = 0.542
E
CD8.CD69
%CD45+CD8+CD69+
p.adj = 0.016
H
Brain-Saline
Brain-BTE
CD44+CD62L- 46.6%
CD44+CD62L+ 15.9%
CD44-CD62L- 3.03%
CD44-CD62L+ 34.5%
CD44+CD62L- 83.9%
CD44+CD62L+ 11.6%
CD44-CD62L- 1.73%
CD44-CD62L+ 3.39%
CD44_BV786-A
CD62L_BUV615-A
G
CD8 Tissue Resident Memory
%CD45+CD8+CD44+CD62L-CD103+
p.adj = 0.022

Figure 4

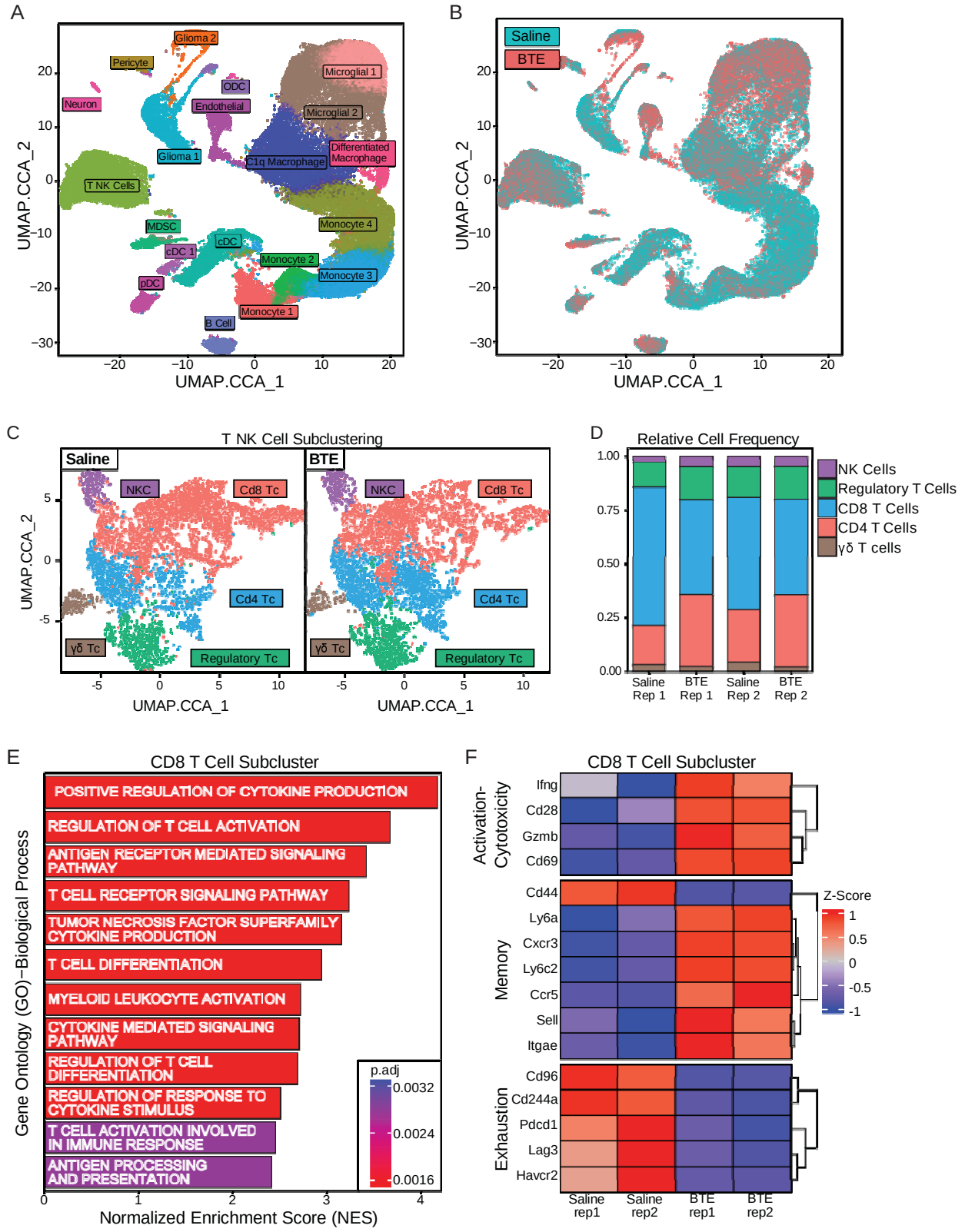
A
Glioma 2
Pericyte
Neuron
ODC
Endothelial
Microglial 1
Microglial 2
Differentiated Macrophage
C1q Macrophage
Glioma 1
T NK Cells
MDSC
cDC
cDC 1
pDC
Monocyte 4
Monocyte 2
Monocyte 3
Monocyte 1
B Cell
UMAP.CCA_2
UMAP.CCA_1
B
Saline
BTE
UMAP.CCA_2
UMAP.CCA_1
C
T NK Cell Subclustering
Saline
BTE
NKC
Cd8 Tc
Cd4 Tc
γδ Tc
Regulatory Tc
UMAP.CCA_2
UMAP.CCA_1
D
Relative Cell Frequency
NK Cells
Regulatory T Cells
CD8 T Cells
CD4 T Cells
γδ T cells
Saline Rep 1
BTE Rep 1
Saline Rep 2
BTE Rep 2
E
CD8 T Cell Subcluster
POSITIVE REGULATION OF CYTOKINE PRODUCTION
REGULATION OF T CELL ACTIVATION
ANTIGEN RECEPTOR MEDIATED SIGNALING PATHWAY
T CELL RECEPTOR SIGNALING PATHWAY
TUMOR NECROSIS FACTOR SUPERFAMILY CYTOKINE PRODUCTION
T CELL DIFFERENTIATION
MYELOID LEUKOCYTE ACTIVATION
CYTOKINE MEDIATED SIGNALING PATHWAY
REGULATION OF T CELL DIFFERENTIATION
REGULATION OF RESPONSE TO CYTOKINE STIMULUS
T CELL ACTIVATION INVOLVED IN IMMUNE RESPONSE
ANTIGEN PROCESSING AND PRESENTATION
p.adj
0.0032
0.0024
0.0016
Gene Ontology (GO)−Biological Process
Normalized Enrichment Score (NES)
F
CD8 T Cell Subcluster
Activation-Cytotoxicity
Ifng
Cd28
Gzmb
Cd69
Memory
Cd44
Ly6a
Cxcr3
Ly6c2
Ccr5
Sell
Itgae
Exhaustion
Cd96
Cd244a
Pdcd1
Lag3
Havcr2
Z-Score
Saline rep1
Saline rep2
BTE rep1
BTE rep2

Figure 5

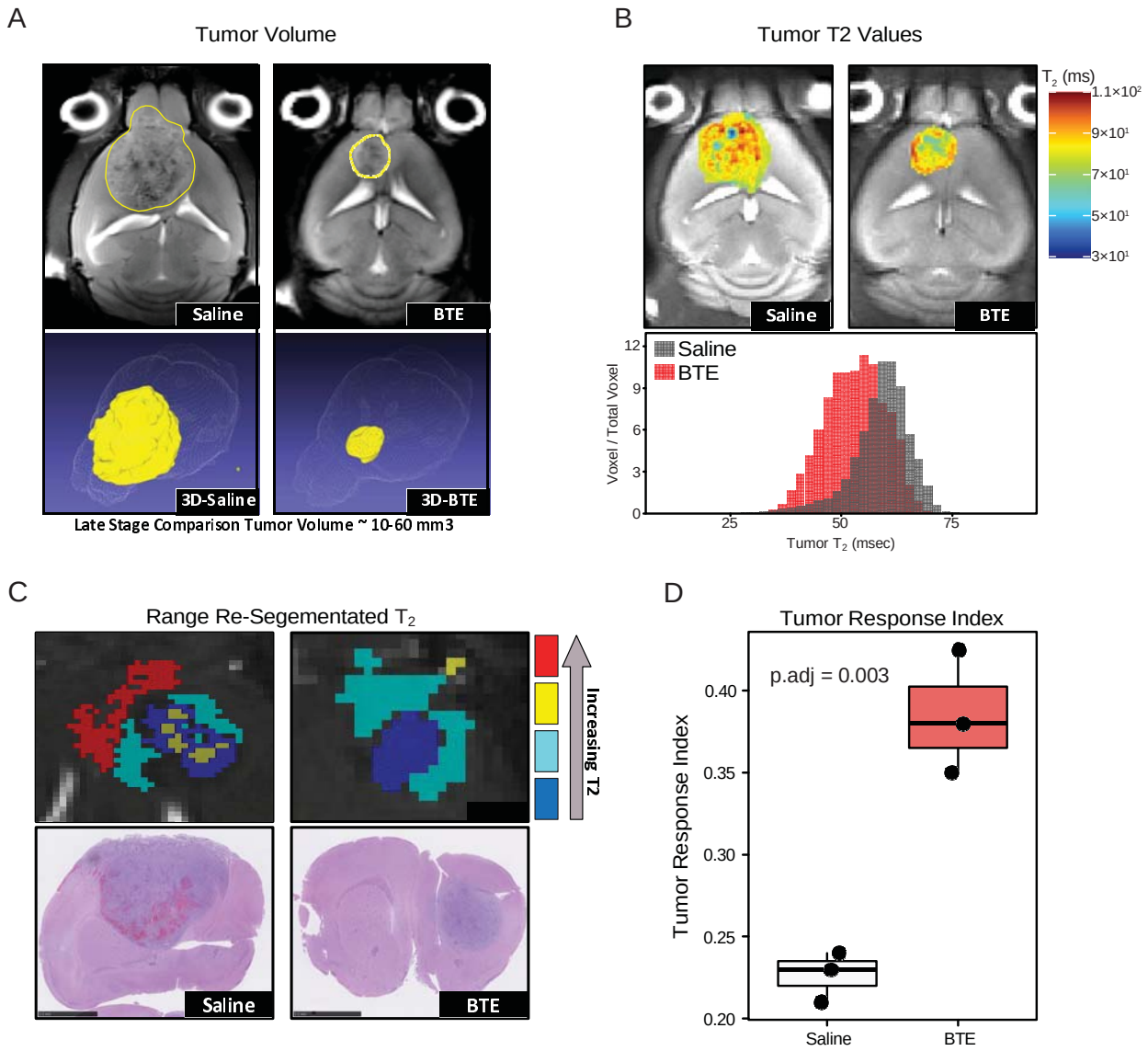
A
Tumor Volume
Saline
BTE
3D-Saline
3D-BTE
Late Stage Comparison Tumor Volume ~ 10-60 mm3
B
Tumor T2 Values
T2 (ms)
1.1×10²
9×10¹
7×10¹
5×10¹
3×10¹
Saline
BTE
Saline
BTE
Voxel / Total Voxel
Tumor T2 (msec)
C
Range Re-Segementated T2
Increasing T2
Saline
BTE
D
Tumor Response Index
p.adj = 0.003
Tumor Response Index
Saline
BTE

Figure 6